Journal of Nuclear Materials 377 (2008) 189–194

Contents lists available at ScienceDirect

Journal of Nuclear Materials

journal homepage: www.elsevier.com/locate/jnucmat

Effect of wettability on bubble formation at gas nozzle under stagnant condition

Hiroyuki Kogawa [a,*], Takahisa Shobu [b], Masatoshi Futakawa [a], Ahmed Bucheeri [c], Katsuhiro Haga [a], Takashi Naoe [c]

[a] Neutron Facility Group, Japan Atomic Energy Agency, Tokai-mura, Ibaraki-ken 319-1195, Japan
[b] Advanced Beam Line Development Group, Japan Atomic Energy Agency, Sayo-cho, Hyogo-ken 679-5148, Japan
[c] Ibaraki University, Hitachi-shi, Ibaraki-ken 316-8511, Japan

A B S T R A C T

Injection of gas microbubbles into mercury might be effective to mitigate pressure waves generating and propagating in liquid mercury target for MW-class spallation neutron sources. The effect of mitigation is very dependent on the bubble conditions; size, population, etc. It is important to make clear bubble formation behavior from a nozzle for development of making suitable gas microbubbles into mercury. Visualization of microbubbles in mercury was carried out by refraction-enhanced imaging with high-energy synchrotron radiation X-rays at SPring-8 to observe the bubble formation behavior at micro-gas nozzle of 100 μm in inner diameter and 200 μm in outer diameter. The bubble formation behavior in mercury was quite different from that in water. A constant taking account of the wettability and interfacial tension force between liquid and solid metals in an equation of force balance around bubble was identified by visualized bubble size. The bubble size under mercury flowing condition was estimated from the force balance equitation.

1. Introduction

The Japan Atomic Energy Agency (JAEA) is currently building the Japan Proton Accelerator Research Complex (J-PARC) project together with the High Energy Accelerator Organization (KEK) [1]. An intense pulsed spallation source called the Japan Spallation Neutron Source (JSNS) is installed in the Material and Life Science Facility (MLF) of J-PARC. In pulsed spallation neutron source, high-energy protons bombard a heavy metal target and neutrons are produced by spallation reaction. The produced high flux neutrons are used for mainly neutron scattering experiments on materials and life sciences. In JSNS, pulsed protons (3 GeV, 1 MW at 25 Hz, 1 μs pulse duration) bombard a liquid mercury target. This liquid metal target material has advantages with heat removal by virtue of its ability to be circulated as well as high neutron yield.

At the moment the protons bombard the target pressure waves are generated in the mercury due to thermal shock [2,3]. The pressure waves will stress the target containment vessel and can cause cavitation erosion damage (pitting damage) [4–8]. The JSNS target vessel is made from type 316LN stainless steel (SS316LN). High fatigue stress and excessive pitting damage are concerns for shortening the life of the target vessel.

The pressure waves should be mitigated to reduce the stress and the cavitation erosion damage in the target vessel. It was numerically suggested that the gas microbubbles injection into the mercury was effective to mitigate the pressure waves but this is very dependent on bubble conditions, i.e., on bubble size and population. For an example in the JSNS target, the initial peak pressure generated at the proton beam center could be reduced from 80 MPa to 40 MPa by introducing gas microbubbles 100 μm in diameter and 10^{-4} in volume fraction [9].

Bubble generating technology in mercury needs development to obtain a suitable bubble size that sufficiently mitigates the pressure waves. Generally, many kinds of bubble injection methods have been developed for the conventional liquid, e.g., water. Examples include injecting gas from micro nozzles; tearing macrobubbles into microbubbles by violent liquid flow; forming microbubbles from gas saturated pressurized liquid by abrupt pressure release. Such bubble generating technologies have been used in the purification of water, food process and chemical engineering processes, etc. [10].

Bubble formation is affected by wettability and interfacial tension force at the interface between liquid and solid (gas–nozzle wall). The effects of wettability and surface tension are quite different between liquid metal and any conventional liquids such as water. These characteristics affect the microbubbles formation, i.e., size of bubble produced. Literature related to the bubblers or bubble behavior in the liquid metals is sparse due to their opacity. Nevertheless, Sano et al. showed that a bubble of about 4 mm in diameter was formed when injecting gas into mercury from a nozzle of 1.7 mm in inner diameter and 2.7 mm in outer diameter and also derived an empirical equation for the bubble size. Because of the poor wettability of mercury, the estimated bubble diameter

* Corresponding author. Tel.: +81 29 282 5074; fax: +81 282 6712.
E-mail address: kogawa.hiroyuki@jaea.go.jp (H. Kogawa).

0022-3115/$ - see front matter © 2008 Elsevier B.V. All rights reserved.
doi:10.1016/j.jnucmat.2008.02.077

generated in the mercury agreed well with the experimental work only when the bubble was assumed to leave from the outer surface of the nozzle as opposed to the inner surface which is appropriate for water [11]. Takahashi et al. derived an equation to estimate the bubble size formed in the water taking account of the force balance around the bubble in the range of bubble size more than a few millimeters [12], so-called meso-bubble, which is relatively larger than that for the mitigation by microbubbls, i.e., 10–100 μm. The equation is helpful for understanding bubble formation behavior in mercury even with its poor wettability compared with conventional liquids, such as water. It can also be used to estimate the bubble sizes formed at the tip of nozzles sized for gas microbubble technology development for pressure wave mitigation.

Full field imaging microscopy is now widely used in the hard X-ray region for observing internal structures of heavy element materials. Especially, the advent of high-energy third-generation synchrotron radiation light sources such as the Super Photon ring-8 GeV (SPring-8) has enabled utilization of high brilliance X-ray beam in high-energy region [13].

An experiment to visualize microbubbles in mercury formed at the tip of a micro-gas nozzle was carried out by using a high-energy X-rays at SPring-8. This paper describes the experiment and the observations of bubble formation, and applies those observations to understand the effect of the wettability on the bubble formation in mercury and for estimating bubble size considering the mercury's poor wettability and the interfacial tension force between mercury and nozzle material.

2. Experimental

2.1. X-rays at SPring-8

The experiment has been carried out at the undulator beamline BL20XU at SPrnig-8. Fig. 1 shows transmission of X-rays in the mercury and acrylic resin obtained by calculation. The transmission ratio increases with the energy of X-rays. However, there is a K-absorption edge at 83.1 keV for mercury because X-rays at this energy excites electrons in the mercury atom. Also, the intensity of X-rays at SPring-8 rapidly decreases over about 100 keV [13]. Therefore X-rays of 82 keV, which have the highest transmission ratio below 100 keV, were used for the visualization experiment from the viewpoint of maximizing intensity of transmitted X-rays.

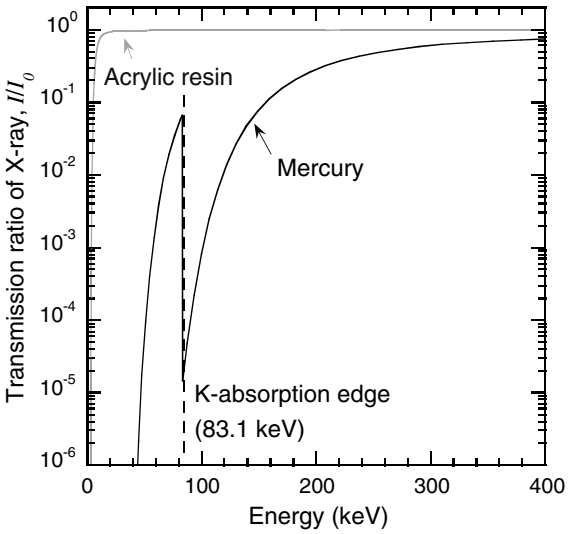

Fig. 1. Transmission ratio of X-rays.

As for the acrylic resin, the transmission ratio is almost 1 over 50 keV.

Fig. 2 shows an attenuation of intensity of 82 keV-X-rays in mercury obtained by calculation. The intensity attenuates to 0.48% of injected intensity when passing through mercury of 2 mm in thickness while it is 77% in the acrylic resin of 10 mm in thickness. However resolution and contrast to sufficiently recognize gas microbubbles depend not only on X-ray intensity but also on properties of the camera used to take the image of the gas microbubbles. Therefore a preliminary test was carried out to optimize the condition of the testing apparatus, including thickness of mercury and acrylic container, and to verify the detectable bubble size. Fig. 3 shows the photograph of the experimental setup at BL20XU. An X-ray Charge Coupled Device (CCD) camera was positioned 5 m behind a sample in order to obtain the visualization image of bubble in the mercury by refraction-enhanced imaging. The X-ray CCD camera used in this experiment can resolve the difference of about 0.15% in contrast. As shown in Fig. 2, since the intensity of X-rays attenuates to 0.48% and 0.63% of injected intensity when passing through mercury of 2 mm and 1.9 mm of mercury, respectively, the corresponding difference of the intensity of X-rays is 0.15%. Therefore, it was estimated that a bubble of 100 μm in diameter could be visualized in 2 mm of mercury.

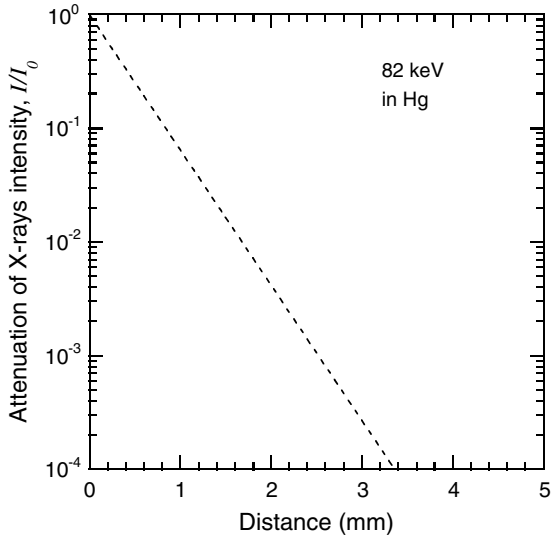

Fig. 2. Attenuation of intensity of X-rays of 82 keV in the mercury and acrylic resin.

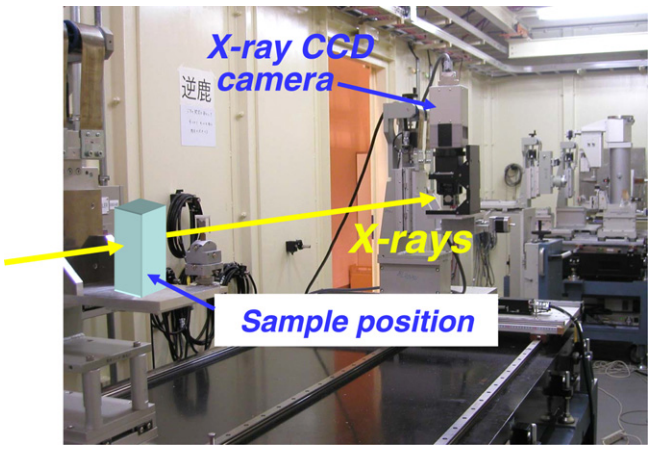

Fig. 3. Experimental setup at SPring-8.

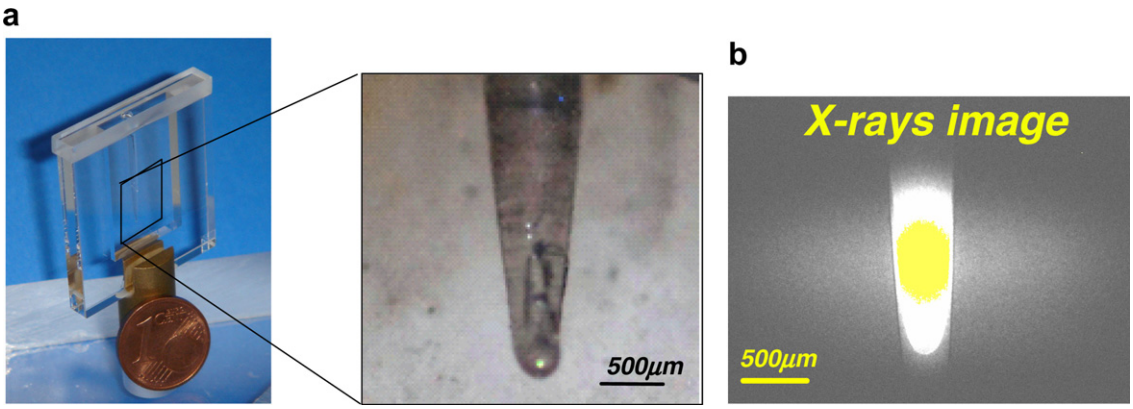

Fig. 4. Preliminary test at SPring-8. (a) Acrylic container with needle, and (b) Visualization result by X-rays.

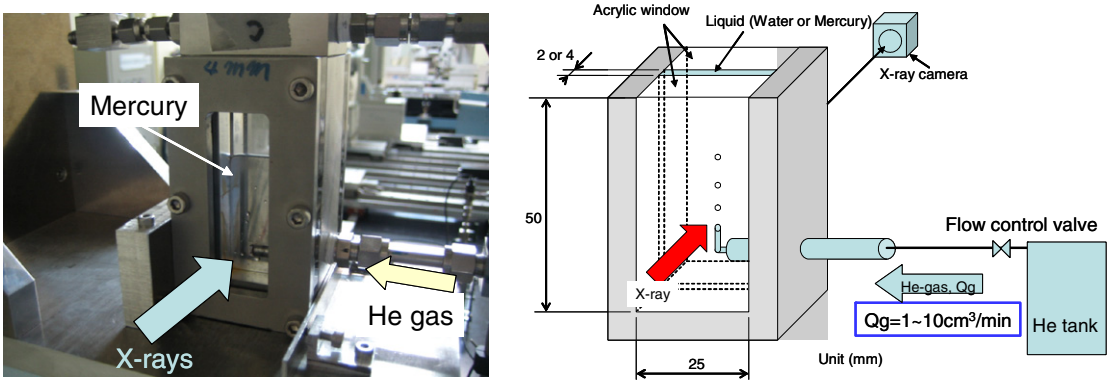

Fig. 5. Schematic drawing of mercury vessel.

Fig. 4(a) shows a mercury container with a glass needle to simulate a gas bubble used for the preliminary test. The mercury thickness of this container was 2 mm which was the same thickness with the vessel used for the bubble visualization as mentioned later. The container was made of acrylic resin. The diameter of glass needle varied gradually to examine the visualization on bubbles with various sizes. Fig. 4(b) shows visualization image taken by X-rays of 82 keV when the container was filled with mercury. The needle part appeared in white in the image thus confirming a gas bubble of order hundreds micro-meter in diameter could be visualized in the mercury of 2 mm in thickness.

2.2. Experimental set-up

Microbubbles of 100 μm and less in diameter might be suitable for pressure mitigation [9]. This experiment's aim was to visualize the behavior of microbubble of 100 μm order in diameter from the needle of 100 μm in inner diameter. Helium gas was injected through a lance type bubbler into mercury which was contained in a vessel. Fig. 5 shows a schematic drawing of the vessel used in the experiment. The vessel was made of acrylic resin to transmit the X-rays and to clearly observe the bubbles in the case that water replaces mercury for another experiment. The attenuation of the X-rays in the acrylic resin was negligible as mentioned above. The size of the vessel cavity is 75 mm in height, 25 mm in width. As for the thickness of mercury through which the X-rays transmit, two vessels were used. One was built for 2 mm and another one for 4 mm mercury thickness. To visualize the smallest bubbles (100 μm ~ a millimeter in diameter) the vessel of 2 mm in thickness was more suitable. However, for the bigger bubbles (millimeter order in diameter bubbles) would easily stick to the wall in the vessel of 2 mm in thickness so it was difficult to measure those sizes. The vessel of 4 mm in mercury thickness was better for observation of bigger bubbles.

At the bottom of the two vessels, a lance type narrow nozzle was installed. Fig. 6 shows the lance installed in the vessels. The used lance was of 100 μm in inner diameter and 200 μm in outer diameter and made of stainless steel. Helium gas was injected into mercury from the exit of the lance. Flow rate of the helium gas was controlled by a needle valve set on the helium gas supplying line.

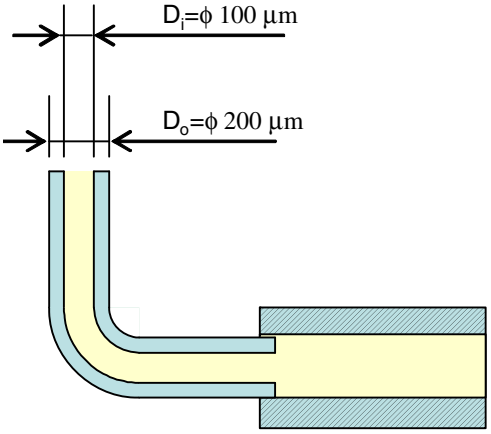

Fig. 6. Narrow nozzle installed into the mercury vessel.

Helium gas ejected from the mercury was vented from the top of the vessel through a mercury vapor filter.

To compare bubble generation behavior in mercury versus water, experiments using water were also carried out. The bubbles generated in water were observed by using a high-speed camera; frame rate was 250 frames per second.

3. Results

Fig. 7 shows a bubble generated in water at the exit of the lance observed by the high-speed camera. Since the lance used for this test was thin, soft and low stiffness, the lance had bent when the lance was installed into the vessel. Consequently the lance inclined 15° to vertical. The bubble grew from the exit of the lance. In comparison, Fig. 8 shows the generated bubble in the mercury around the exit of the lance observed by X-rays in the case of the vessel of 2 mm in thickness. The bubble formation in mercury was different from that in water; the bubble grew surrounding the lance. This suggests that the difference between bubble generation in water and mercury was greatly affected by the wettability between liquid and the surface of lance.

Fig. 9 shows the bubble growing behavior after the situation shown in Fig. 8 in the mercury in the case of the vessel of 4 mm in thickness. The bubble grew up surrounding the outer surface of the lance in a spherical like shape as shown in Fig. 9(a) and (b) as well as Fig. 8. Later, necking was observed as shown in Fig. 9(c). From these observations, it is understood that the bubble grows on the outer surface of the nozzle in the mercury.

Fig. 10 shows the bubble diameter measured from the images taken by X-rays at SPring-8. The bubble diameter seemed constant independently of the gas flow rate. Fig. 10 also shows the results by Sano et al. [11] for relationship between the gas flow rate and bubble diameter generated from a lance of 1.7 mm in inner diameter and 2.7 mm in outer diameter. These bubble diameters were estimated from ratio of the gas flow rate to the bubble formation frequency. The bubble formation frequency was measured by piezoelectric sensor to catch rapid pressure change in the lance due to the bubble detachment from the lance. The bubble diameter generated in mercury was almost constant in low gas flow rate region, less than 20 cm^3/min and the bubble diameter was ca. 4 mm. In the present work, a narrow lance was used; 100 μm in inner diameter and 200 μm in outer diameter. The bubble diameter became ca. 2 mm for this smaller lance independently of the gas flow rate.

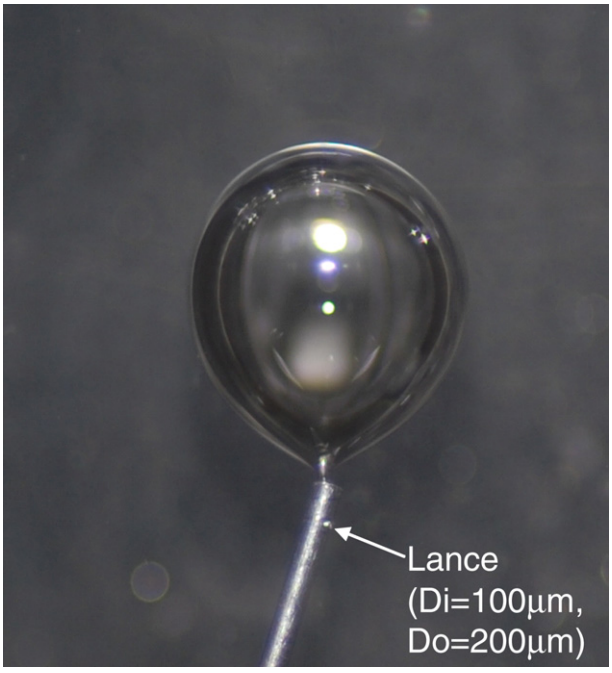

Fig. 7. Bubble generated in water at the exit of the lance.

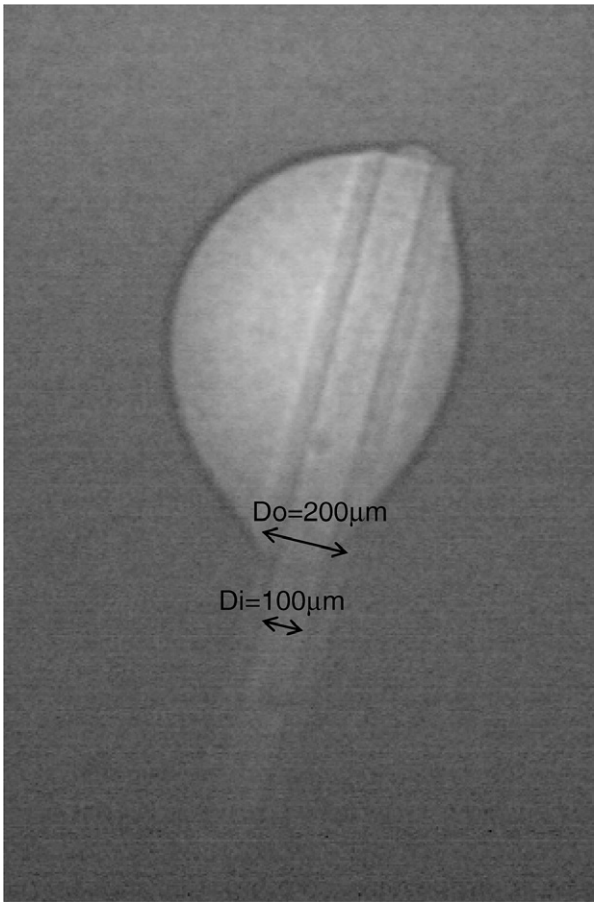

Fig. 8. Refraction-enhanced image of bubble generated in mercury at the exit of the lance.

4. Discussion

As shown in Fig. 9, the bubble grew with a spherical shape at first, and then the necking part appeared. The bubble growing behavior seems to be expressed in two stages as shown in Fig. 11. Wettability is represented by contact angle. The contact angle between the mercury and nozzle material is large because of poor wettability of mercury to the nozzle material. The contact point between bubble and solid grow away from the center of the bubble to keep constant contact angle when the bubble is growing as shown in the first stage of Fig. 11. After the contact point reaches the corner of the lance, bubble is growing as surrounding the outer surface of the lance to keep constant contact angle as shown in Fig. 8. While, the bubble in the water can grow keeping constant contact angle and contact point because the contact angle between water and solid is small.

The bubble size is very important to realize the pressure wave mitigation. Takahasi et al. calculated the generated bubble in water by solving the force balance equation among a inertia forces, buoyancy, drag, and interfacial tension forces assuming a 2stage model in a cocurrent flowing water [12]. At the end of the first stage, the force balance equation is expressed as follows:

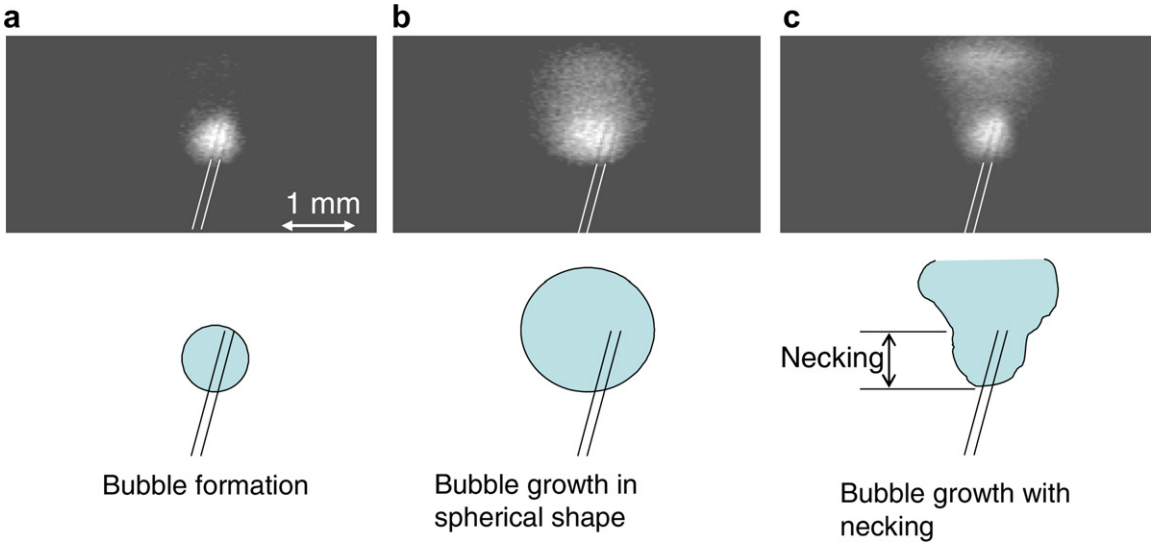

Fig. 9. Bubble growing behavior in the mercury at the narrow nozzle.

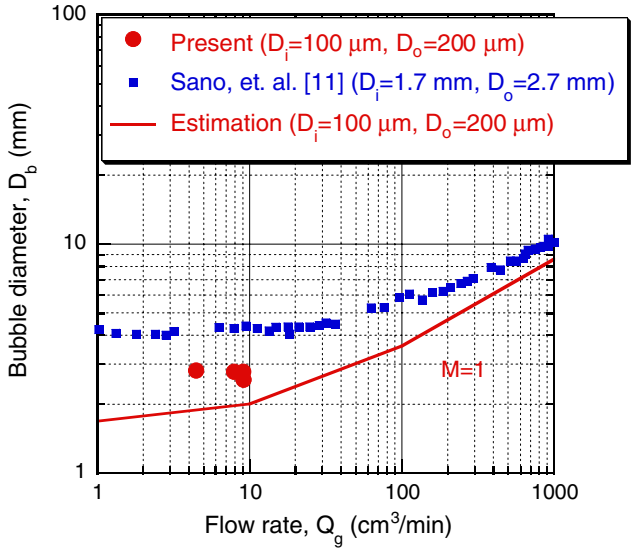

Fig. 10. Relationship between the bubble diameter generated in mercury and gas flow rate.

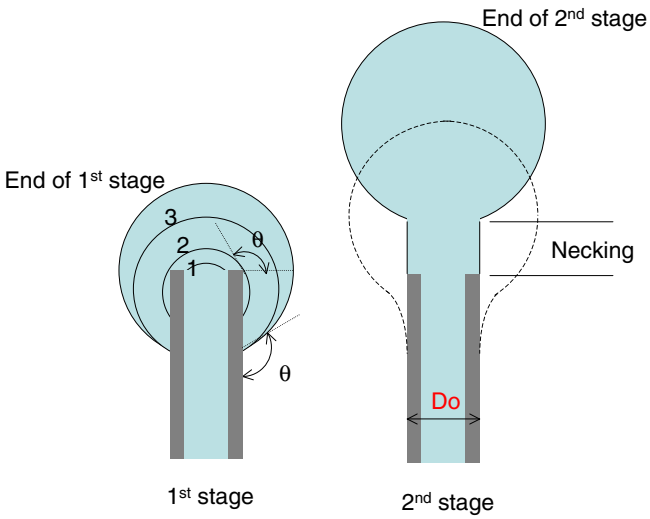

Fig. 11. Schematic drawing of the 2-stage model.

$$\frac{d[(11\rho_L V_f/16)(v-U_L)]}{dt} = \rho_L V_f g - \frac{C_D \pi R_f^2 \rho_L}{2}(v-U_L)|v-U_L| - M\pi D_i \sigma,$$
$$V_f = \frac{4}{3}\pi R_f^3,$$
$$C_D = 1 + 16/Re,$$
$$Re = \frac{2R_f v}{\nu}, \quad (1)$$

where, ρ_L is density of liquid, V_f the volume of the gas bubble at the end of the first stage, v velocity of bubble center, U_L the velocity of liquid, R_f the radius of bubble at the end of the first stage, D_i the inner diameter of lance, σ the surface tension of liquid, ν the kinematic viscosity of liquid and M the constant to express interfacial tension force between the liquid and solid metal. At the second stage, the force balance is expressed as follows:

$$\frac{d[(11\rho_L V_b/16)(v'-U_L)]}{dt_s} = \rho_L(V_f + Q_g t_s)g - \frac{C_D \pi R_b^2 \rho_L}{2}(v'-U_L)|v'-U_L| - M\pi D_i\sigma, \quad (2)$$

$$v' = \frac{ds}{dt_s},$$

where, s is the length of necking. Eq. (2) is solved by assuming that the bubble leaves the lance at $s = [3V_{f0}/(4\pi)]^{1/3}$, where V_{f0} is the volume of the gas bubble at the end of the first stage in stagnant liquid.

In the present data, the generated bubble diameter did not depend on the flow rate, similarly as in Sano's data in the low gas flow rate region; $Q_g < 20$ cm^3/min. At low gas flow rate, since the bubble growth rate is very slow, the inertia force and the drag force become negligible small. Then, Eq. (1) can be rewritten in Eq. (3) for the low gas flow rate region as the case of the present test,

$$D_b = \left(\frac{6M\sigma D_i}{\rho g}\right)^{1/3} \quad (3)$$

The third term of the right hand in Eqs. (1) and (2) shows the interfacial tension force between the liquid and solid. The interfacial tension force would depend on the interface condition such as the wettability as well as the surface tension. In the estimation, the effect of the interface condition is noted by M value. The empirical equations have been proposed for the bubble diameter generated in the water at low gas flow rate. The form of the empirical

equations is the same as Eq. (3) but M value is different. In the empirical equations, M varied from 0.79 to 9.145 [14–16]. Fig. 12 shows the bubble diameter calculated by Eq. (3) against M value. In the calculation, the inner diameter, D_i, replaced the outer diameter, D_o = 200 μm, since the bubble was generated from the outer surface of the lance in the mercury as shown in Figs. 8, and 9. Since the generated bubble in the present test were in 2.5–2.8 mm range, the estimation by Eq. (3) agrees with the present data when M value is 3.9–4.8. The lance inclined 15°. This inclination increases projected outer diameter to horizontal plane only 3.5%. So this hardly has an influence on the generated bubble diameter.

As shown in Fig. 9, necking was observed in bubble growth. Then, the 2-stage model was used as expressed by Eqs. (1) and (2) to estimate the bubble diameter. Since the bubble was generated from the outer surface of the lance in the mercury as shown in Figs. 8 and 9, the inner diameter, D_i, in Eqs. (1) and (2) replaced by the outer diameter, D_o. The estimated bubble diameter is plotted in Fig. 13 when the M value is 4.5 in Eqs. (1) and (2). The estimated bubble diameter by 2-stage model agrees well with the experimental.

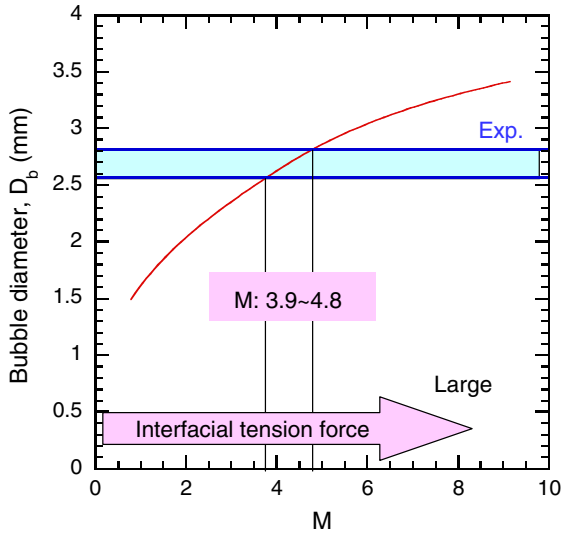

Fig. 12. Relationship between the generated bubble diameter in the mercury and M value related to the wettability in the empirical equation.

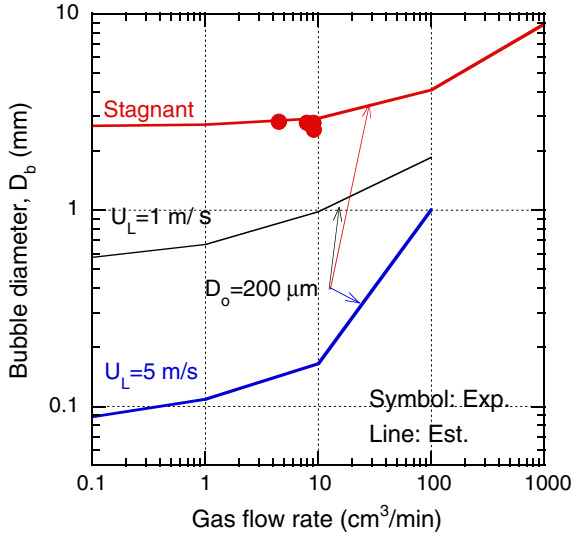

Fig. 13. Estimated bubble diameter by using 2-stage model.

To make smaller bubbles, the effect of the mercury flow to upward was considered due to a drag force become to load upward as shown in Eqs. (1) and (2). The bubble diameter under the mercury flow condition was estimated from Eqs. (1) and (2) and shown in Fig. 13. In this estimation, 4.5 was used for M value and mercury flow velocity, U_L, was set to 1.0 m/s which is equal to the estimated mercury flow velocity in the JSNS mercury target. The generated bubble diameter was decreased to 570 μm when the gas flow rate is 0.1 cm^3/min.

In the JSNS mercury target, flow velocity of mercury would be increased up to 5 m/s by taking care of degradation of the target vessel by erosion induced by mercury flow. The generated bubbles of 110 μm and 165 μm in diameter could be realized at 1 cm^3/min and 10 cm^3/min of gas flow rate, respectively.

5. Conclusion

Bubble formation from a narrow lance (D_i = 100 μm, D_o = 200 μm) was visualized by using X-rays at SPring-8.

Bubble behavior around the lance in the mercury is obviously different from that in water because of the difference in wettability; the bubble grows surrounding the lance in mercury due to the poor wettability though it grows at the top of the lance in water.

The estimated bubble diameter using 2-stage model agreed well with the experimental taking into account that the bubble left from the outer surface of the lance in mercury and the interfacial tension force between the mercury and the lance.

The generated bubble diameter from a lance of 200 μm in outer diameter was predicted to be 110 μm, which would be effective on the pressure wave mitigation, under the conditions of the mercury flow of 5 m/s and gas flow rate of 1 cm^3/min from the estimation of the 2-stage model.

Acknowledgements

We would like to thank Dr Y. Suzuki and Dr A. Takeuchi of the Japan Synchrotron Radiation Research Institute (JASRI) for technical support through the experiments. The synchrotron radiation experiments were performed at the BL20XU in SPring-8 with the approval of JASRI (Proposal No. 2006A1387-NL-np). This work was supported by Japan Society for the Promotion of Science under Grant-in-Aid for Scientific Research 17360085.

References

[1] Planning Division for Neutron Science, in: Proceedings of the 3rd Workshop on Neutron Science Project – Science and technology in the 21st century opened by intense spallation neutron source, JAERI-Conf 99-003, 1999.
[2] H. Kogawa, et al., in: Proceedings of the ICANS-XVI, vol. III, 2003, p. 1925.
[3] S. Ishikura, H. Kogawa, M. Futakawa, R. Hino, H. Date, Kouongakkaishi 28 (6) (2002) 329 (in Japanese).
[4] M. Futakawa, H. Kogawa, R. Hino, J. Phys. IV France 10 (2000) Pr9-237.
[5] M. Futakwa, H. Kogawa, Y. Midorikawa, R. Hino, H. Date, H. Takeishi, in: Proceedings of the 4th International Symposium on Impact Engineering, 2001, p. 339.
[6] M. Futakawa, H. Kogawa, R. Hino, H. Date, H. Takeishi, Int. J. Impact Eng. 28 (2003) 123.
[7] M. Futakawa, T. Naoe, H. Kogawa, C.C. Tsai, Y. Ikeda, J. Nucl. Sci. Technol. 40 (2003) 895.
[8] M. Futakawa, T. Naoe, C.C. Tsai, H. Kogawa, S. Ishikura, Y. Ikeda, H. Soyama, H. Date, J. Nucl. Mater. 343 (2005) 70.
[9] K. Okita, S. Takagi, Y. Matsumoto, Nihon Kikai Gakkai Ronbunsyu B 72 (716) (2006) 885 (in Japanese).
[10] "Concept of Basic Bubble and Foam Engineering", Tekunosisutemu, Tokyo, 2005, pp.421-484. (in Japanese).
[11] M. Sano, K. Mori, T. Sato, Tetsu to Kou 60 (3) (1974) 348 (in Japanese)..
[12] T. Takahashi et al., Kagaku Kougaku Ronbunshu 6 (1980) 563.
[13] <http://www.spring8.or.jp/en/users/new_user/sr/feature/>.
[14] T. Tadaki, S. Maeda, Kagaku Kougaku 27 (1960) 147.
[15] C. Maier, US Bur. Mines Bull. (1927) 260.
[16] W. Siemes, Chem. Eng. Sci. 5 (1956) 127.